Relative density estimation from shallow depth CPTs in siliceous sand: an updated approach

Mathias Rolf Jensen[1] BE, MSc

[1]Corresponding author
Geotechnical Engineer,
Geo, Copenhagen, Denmark
Maglebjergvej 1, 2800 Kongens Lyngby
Phone +45 3174 0205
Email: mtj@geo.dk

Abstract

Cone penetration tests (CPTs) in sands are governed by two distinct mechanisms: a shallow failure mode, which dominates in the upper ~0.2–1.0 m of standard field CPTs, and a deep failure mode, which develops once sufficient embedment is achieved. Industry-standard correlations between CPT cone resistance (q_c) and relative density (D_r) are calibrated under deep failure conditions, and their application in the shallow zone produces erroneous results. This paper reviews existing shallow depth interpretation methods and introduces an updated global model integrating shallow and deep penetration mechanisms. Building on Jensen (2024), the new formulation addresses prior limitations through comprehensive recalibration using controlled laboratory tests and a database of 132 onshore and offshore CPTs, enabling improved differentiation of near-surface densities and closer agreement with measured q_c profiles. The model shows significant reduction in shallow-zone D_r bias relative to earlier approaches and is most reliable for clean, young, uncemented, uniformly graded siliceous sands under fully saturated or dry conditions. Deviations occur in sands of higher compressibility, increased fines content, or pronounced angularity, and within the top 2–4 cone diameters where mudline definition and minor cone disturbance become influential. Site-specific validation of the model against direct D_r measurements is required for reliable application, even within the calibrated range.

Revised version submitted to Geotechnical Research (status: minor revision)

Keywords

CPT; cone resistance; sands; shallow depth; relative density.

List of notations

φ'	Peak friction angle
φ'_{cs}	Critical state friction angle
γ'	Effective unit weight
σ'	Normalizing effective stress
σ'_h	Horizontal effective stress
σ'_p	Preconsolidation stress (Fig. 7)
σ'_v	Vertical effective stress
σ_v	Vertical total stress
a	Empirical fitting parameter (Eqs. (7) & (10))
d_c	Cone diameter
$C_{0.deep}$	Empirical fitting parameter (Eqs. (2) & (3))
$C_{1.deep}$	Empirical fitting parameter (Eqs. (2) & (3))
$C_{2.deep}$	Empirical fitting parameter (Eqs. (2) & (3))
$C_{0.shallow}$	Empirical fitting parameter (Eq. (6))
$C_{1.shallow}$	Empirical fitting parameter (Eq. (6))
$C_{2.shallow}$	Empirical fitting parameter (Eq. (6))
CPT	Cone penetration test
D_r	Relative density
$D_{r.deep}$	Predicted relative density considering deep failure penetration
$D_{r.shallow}$	Predicted relative density considering shallow failure penetration
e_{max}	Maximum void ratio
e_{min}	Minimum void ratio
$f_{transition}$	Transition function (Eq. (9))
K	Lateral stress coefficient (Eg. (4))
K_0	Coefficient of earth pressure at rest
m'	Stress exponent (Fig. 7)
n_1	Fitting parameter (Eq. (9))
n_2	Fitting parameter (Eq. (9))
N_q	Bearing capacity factor (Eq. (4))
NC	Normally consolidated
ND	Nuclear densometer
OC	Overconsolidated
OCR	Overconsolidation ratio

p_a	Reference stress (=100 kPa)
p'	Mean effective stress
PSD	Particle size distribution
q_c	Cone resistance
$q_{c.deep}$	Predicted cone resistance considering deep failure penetration
$q_{c.global}$	Predicted cone resistance considering both shallow and deep failure penetration
$q_{c.shallow}$	Predicted cone resistance considering shallow failure penetration
UC	Uniformity coefficient
z	Depth of penetration
q_t	Corrected cone resistance (Fig. 7)
z_{cr}	Critical depth
z/d_c	Normalized penetration depth

Introduction

When sufficient embedment is achieved during cone penetration in sand, a deep failure mechanism develops, characterized by a localized deformation zone near the cone tip (Arshad et al., 2014). Deep penetration has been widely analyzed using the analogy between cone penetration and spherical cavity expansion (e.g., Salgado and Prezzi, 2007). In contrast, the upper ~0.2-1.0 m of standard field cone penetration tests (CPTs) is typically governed by a shallow failure mechanism, associated with upward displacement of surface sand (Biarez and Gresillon, 1972). A transition zone separates the shallow and deep mechanisms, marking a shift in the governing soil deformation pattern (Puech and Foray, 2002).

Industry-standard methods for estimating the relative density (D_r) of sand from CPT cone resistance (q_c) are largely empirical, based on CPTs in calibration chambers under deep failure conditions (e.g., Baldi et al., 1986; Jamiolkowski et al., 2003). Applying these methods to near-surface sands, where shallow failure governs, leads to erroneous D_r estimates. Accurate estimation of relative density at shallow depths is of practical importance in various geotechnical applications. Near-surface sands often control the performance of shallow foundations, pipelines, cables, and earthworks. Erroneous classification of shallow sand as loose, when it is in fact dense, may lead to overly conservative designs, unnecessary ground improvement, or incorrect assessment of serviceability performance. Conversely, overestimation of D_r may result in unconservative predictions of foundation performance.

Despite its practical importance, guidance for interpreting CPT data at shallow depths remains limited. Although several researchers have advanced understanding of shallow failure penetration and the transition zone (Puech and Foray, 2002; Emerson et al., 2008; Kim et al., 2015; Lehane et al., 2022; Jensen, 2024), these developments have not yet been widely incorporated into routine engineering. This paper provides a critical review of existing methods for estimating D_r at shallow depths and introduces an updated global model that extends the formulation of Jensen (2024).

While Jensen (2024) introduced a unified framework for combining shallow and deep penetration mechanisms, the initial calibration of the model exhibited limitations in the very near-surface zone and was based on a small dataset. The present study addresses these limitations through recalibration using comparisons with alternative theoretical and empirical interpretation methods, previously published controlled laboratory tests, field CPTs with measured D_r, and a new database of 132 onshore and offshore CPTs. This approach enables both quantitative validation and broader qualitative evaluation. Refinement of the shallow penetration coefficient and transition function improves predictive performance in the shallow failure zone and reduces bias in near-surface D_r estimation, thereby strengthening the model's practical applicability.

2. Background

2.1 Shallow failure penetration

As illustrated in Fig. 1, cone penetration in uniform sand deposits generally exhibits a transition in the measured cone resistance profile, $q_c(z)$, with depth (z), from a shallow failure mode to a deep failure mode. In the very near-surface zone, shallow failure dominates, producing an upward-concave $q_c(z)$ profile characterized by an increasing gradient (dq_c/dz). The mechanics of shallow failure penetration are governed primarily by the mobilized friction angle and soil dilatancy (Durgunoglu and Mitchell, 1973). This penetration mode has been the subject of several studies (e.g., Puech and Foray, 2002; Balachowski, 2007; Kim et al., 2015).

Experimental observations by Kim et al. (2015), consistent with the general findings of Lehane et al. (2022), indicate that the transition from shallow to deep failure occurs at a depth of penetration of approximately 3-6 cone diameters in loose, clean silica sand, and about 15-20 cone diameters in dense silica sand. Based on their tests, Kim et al. (2015) proposed the following expression with a form that describes the upward-concave $q_c(z)$ profile representative of shallow failure penetration ($q_{c.shallow}$) in clean silica sand:

$$q_{c.shall} \quad = (0.96 \cdot D_r - 0.25) \cdot \left(\frac{\sigma'_v}{p_a}\right)^{0.5} \cdot \left(\frac{z}{d_c}\right) \cdot p_a \tag{1}$$

where p_a is a reference stress (= 100 kPa), σ'_v is vertical effective stress, and d_c is the cone diameter. Following Kim et al. (2015), both $q_{c.shallow}$ and σ'_v are expressed in MPa in Eq. (1). Although this convention may appear dimensionally inconsistent, it is retained to ensure comparability with their formulation. Equation (1), along with other approaches, is discussed further later in this paper.

2.2 Deep failure penetration

At greater depth, the penetration response transitions to a deep failure mode with decreasing dq_c/dz, as shown in Fig. 1. Deep failure penetration is primarily governed by sand compressibility characteristics (Konrad, 1998; Yu and Mitchell, 1998). Widely used CPT-D_r correlations for deep failure are based on Schmertmann's (1976) formulation:

$$q_{c.deep} = C_{0.deep} p_a \left(\frac{\sigma'}{p_a}\right)^{C_{1.deep}} \exp\left(C_{2.deep} D_{r.deep}\right) \tag{2}$$

$$D_{r.deep} = \frac{1}{C_{2.deep}} \ln\left(\frac{q_{c.deep}/p_a}{C_{0.deep}(\sigma'/p_a)^{C_{1.deep}}}\right) \tag{3}$$

where $C_{0.deep}$, $C_{1.deep}$, and $C_{2.deep}$ are empirical fitting parameters, and σ' is the normalizing effective stress.

In normally consolidated (NC) sands, calibration is often performed using the vertical effective stress σ'_v (e.g., Schmertmann, 1978; Baldi et al., 1986). However, Houlsby and Hitchman (1988) demonstrated that the horizontal effective stress (σ'_h) has a stronger influence on q_c. Consequently, many methods adopt the mean effective stress, $p' = (\sigma'_v + 2\sigma'_h) / 3$, improving generality, particularly in overconsolidated (OC) sands where the coefficient of earth pressure at rest (K_o), on which σ'_h depends, is significantly higher (e.g., Jamiolkowski et al., 2003; Krogh et al., 2022).

In the upper 3-5 m of OC sands, where K_o and the overconsolidation ratio (OCR) vary significantly with depth, stress normalization using p' becomes particularly important to avoid overestimation of D_r, as may occur when normalizing solely with σ'_v. Depth-dependent $K_o(z)$ can be evaluated using the approach of Krogh et al. (2022) (procedure given in the flowchart in Fig. 7 presented later in the paper), where preconsolidation stress is estimated following Agaiby and Mayne (2019). Importantly, Emerson et al. (2008) and Jensen (2024) demonstrated that better interpretation of shallow CPT data requires integrating the $K_o(z)$-based stress normalization with shallow failure considerations, as discussed in the following.

3. Review of CPT-based interpretation methods for shallow D_r estimation

3.1 Limit equilibrium method (Puech and Foray, 2002; Emerson et al., 2008)

Puech and Foray (2002) developed a limit equilibrium model for shallow failure penetration in siliceous sand based on bearing capacity theory, incorporating friction angle, cone diameter, and lateral friction:

$$q_{c.shallow} = \gamma' \cdot z \cdot N_q \left(1 + \frac{K \cdot \sin\varphi'}{L} \cdot z\right) \tag{4}$$

where γ' is effective unit weight of sand, φ' the peak friction angle, L is the dimension of a soil cylinder considered around the cone ($L = d_c \cdot \exp(\tan(\varphi' \cdot (\pi/2))) \cdot \tan(\pi/4+\varphi'/2)$), $N_q = 1.058 \cdot \exp(6.168 \cdot \tan\varphi')$, and K is a lateral stress coefficient, different from K_0 and ranging from approximately 1 to 3 (Emerson et al., 2008). Equation (4) is to be applied with curve fitting while relating D_r via the following correlation with φ':

$$\varphi' = 20.4° \cdot D_r + 25° \tag{5}$$

Distinguishing between shallow and deep failure penetration is critical, since deep failure penetration in loose sand can produce q_c-profiles that resemble those from shallow penetration in dense sand, leading to misinterpretation of relative density. To address this issue, Emerson et al. (2008) proposed a global q_c model ($q_{c.global}$) that via a transition function combines Puech and Foray's (2002) model for $q_{c.shallow}$ with the widely applied calibration of deep failure penetration ($q_{c.deep}$; Eq. (3)) by Jamiolkowski et al. (2003); see Table 1. In their global model, the transition between shallow and deep failure penetration is defined by a critical depth (z_{cr}), primarily dependent on D_r; lower D_r causes shallower onset of deep failure.

Figures 2a and 2b show Emerson et al.'s (2008) global model applied to two CPTs at a German test site with homogeneous, clean, uniformly graded, fine to medium OC siliceous sand, using a standard 10 cm^2 cone (d_c = 3.57 cm) (data from Krogh et al., 2022). Nuclear densometer (ND) tests performed at the site indicate D_r = 60% ±10% (CPT-02; Fig. 2a) and D_r = 80% ±10% (CPT-03; Fig. 2b). A weakness in Emerson et al.'s model lies in the parameter K (Eq. (4)), which is somewhat arbitrary. Although K strongly influences the predicted $q_{c.shallow}$ profile in the model, no robust guidance exists for selecting an appropriate value in practice. For comparison within the shallow failure zone, Emerson et al.'s (2008) global model is evaluated against the experimentally derived expression for $q_{c.shallow}$ proposed by Kim et al. (2015) (Eq. (1)). The two approaches show good agreement in the shallow zone when Emerson et al.'s model is applied with $K = 2.5$ (Figs. 2a and 2b). In these comparisons, representative relative density ranges of D_r = 0.6-0.8 (Fig. 2a) and 0.65-0.85 (Fig. 2b) were used, corresponding to the ND test results.

Although the curves now show reasonable agreement with the direct ND measurements of D_r in the shallow zone, Emerson et al.'s model does not accurately capture the transition from shallow to deep failure, predicting the shift at a considerably greater penetration depth than indicated by the CPT data (Fig. 2). Furthermore, the abrupt shift from increasing dq_c/dz (shallow zone) to decreasing dq_c/dz (deep zone) does not fit the general observation of a gradually changing gradient (Fig. 1). If applying a lower value of K, the transition to the deep failure penetration could have been captured better, but that would have then compromised the accuracy significantly in the shallow failure zone. Similar discrepancies were noted by the author comparing with the extensive internal CPT database, presented later in this paper.

3.2 Centrifuge-based model (Lehane et al., 2022)

Centrifuge CPTs, due to limited penetration, are well suited for studying shallow failure penetration (e.g., Bolton et al., 1999; Balachowski, 2007). Lehane et al. (2022) used a large centrifuge database to describe the shallow-to-deep transition with a hyperbolic tangent function:

$$q_{c.shallow} = \tanh\left(\frac{az}{d_c}\right) C_{0.shallow} p_a \left(\frac{\sigma_v'}{p_a}\right)^{C_{1.shall}} \quad \exp(C_{2.shall} \quad D_{r.shall} \quad) \qquad (6)$$

where $C_{0.shallow}$, $C_{1.shallow}$, and $C_{2.shallow}$ are empirical parameters calibrated by Lehane et al. (2022) for clean, uniformly graded, fine to medium, freshly deposited NC silica sands using

$\sigma' = \sigma'_v$ (Table 1), and a is an empirical curve fitting parameter, given by Lehane et al. (2022) as:

$$a = 0.66\exp(-2.5D_{r.shallow}) \tag{7}$$

Equation (7) (Lehane et al., 2022) is shown in Fig. 3 together with the a values derived from their centrifuge database, and supplemented with values inferred by the author from data presented by Puech and Foray (2002) and Emerson et al. (2008) from CPTs performed with a standard 10 cm^2 cone. Although designated "shallow", Eq. (6) may also apply for deep failure penetration in freshly deposited NC sands, since it essentially transitions into a deep failure expression (Eq. (2)) when the tangent hyperbolic function approaches unity with depth, as controlled by the a parameter. In this study, however, it is primarily used to model the shallow zone and the transition.

When applied using D_r = 0.6-0.8 (Fig. 4a) and D_r = 0.65-0.85 (Fig. 4b), predicted q_c values fall well below the field data, with the discrepancy increasing beyond ~0.3-0.4 m, as expected due to overconsolidation effects. Jensen (2024) noted that Eqs. (6) and (7) effectively captures the shape of field q_c profiles in moderately compressible siliceous sands. However, overconsolidation effects influences deep q_c significantly and must be accounted for.

For shallow failure penetration, Jensen (2024) argued that overconsolidation has little, if any, effect on shallow failure penetration resistance. This conclusion was supported by two main pieces of evidence. Firstly, numerical simulations by Krogh et al. (2022) (Fig. 5) demonstrated comparable $q_{c.shallow}$ for relative densities of D_r = 0.65 (Fig. 5a) and D_r = 0.85 (Fig. 5b), under both constant K_0 = 0.414 (representative of NC sand) and depth-dependent K_0(z) (representative of OC sand). Secondly, similar trends can be inferred from the initial penetration curves reported in experimental centrifuge CPT studies by El-Sekelly et al. (2015), Roy (2020), and Richards et al. (2021). These experiments, conducted at varying g-levels, effectively simulated a range of OCR values, including NC conditions.

Building on these observations, Jensen (2024) proposed a global q_c model that combines Eqs. (2) and (6), with the transition governed by OCR (or K_0). An assumption in this approach is therefore that very shallow q_c values are equivalent for both normally consolidated and overconsolidated sands, with OCR effects becoming more pronounced with increasing embedment approaching deep failure penetration.

3.3 Global model (Jensen, 2024)

To capture both failure regimes and the transition, Jensen (2024) proposed:

$$q_{c.global} = \begin{cases} q_{c,shall} & if\ \tanh(az/d_c) \le n_1 \\ q_{c.shallow} + f_{transition}(q_{c.deep} - q_{c.shall}\quad) & if\ \tanh(az/d_c) > n_1 \end{cases} \qquad (8)$$

where

$$f_{transition} = \left(\frac{\tanh\left(\frac{az}{d_c}\right) - n_1}{1 - n_1} \right)^{n_2} \qquad (9)$$

with $n_1 = 0.5$ and $n_2 = 2$ suggested as initial proof of concept values, subject to further calibration. Jensen (2024) also proposed that the calibration of Eq. (6) could be extended to deep failure (Eq. (2)) by making small adjustments to $C_{0.shallow}$, thereby enabling a shift from σ_v' to p' in stress normalization (Table 1).

The global model, defined by Eqs. (8) and (9) and incorporating Jensen's (2024) preliminary calibration, is presented in Figs. 6a and 6b. The predicted $q_{c.global}$ profiles closely match the shape of the measured CPT data and align well with the ND measurements. However, a current key limitation is evident in the upper ~0.4 m: the profiles converge in the initial penetration for the applied D_r range, preventing objective differentiation of D_r. Although the model successfully captures the overall profile shape, this shortcoming highlights the need for refinement, which is addressed in the following section.

4. Updated global model

To support refinement of the global model, an internal database of 132 shallow CPTs from onshore and offshore industry projects was compiled and analysed in conjunction with previously published controlled laboratory tests. The internal database comprises onshore tests conducted in Denmark and Germany, and offshore tests performed in the North Sea and Irish Sea; details are summarized in Table 2. The onshore CPTs were mainly carried out in recently placed, clean siliceous sand fill with varying degrees of compaction, whereas the offshore CPTs were conducted in young, surficial, clean siliceous deposits. As noted in the descriptions for each site (Table 2), the tested sands generally consist of fine to coarse, uniformly graded sand, as confirmed by sampling. Of the total tests, 96 CPTs were performed with a 10 cm^2 cone and 36 CPTs using a 15 cm^2 cone, all from the same site (Site B(2)). Each CPT was advanced to a depth constraining both shallow and deep failure penetration.

A qualitative review of the internal CPT database indicated that the transition to deep failure penetration generally occurs at a slightly shallower depth, particularly for loose to medium dense sands, than predicted by the current model governed by the coefficient a defined in Eq. (7). That is, a controls the hyperbolic tangent function in Eq. (6), which drives the transition of the q_c profile to deep failure penetration as the function approaches unity. To account for this, a minor modification to Eq. (7) is proposed, resulting in an improved fit to the internal database and a closer overall correspondence with the data shown in Fig. 3:

$$a = 0.79\exp(-2.6D_{r.shallow}) \tag{10}$$

The review of the internal database also indicates that Lehane et al. (2022) profiles (Eq. (6)), which forms the basis for the global model by Jensen (2024) in the very shallow zone, consistently underestimate $q_{c.shallow}$ in the near-surface range for both loose and dense sands. This trend is further supported by the distinct discrepancy observed in Fig. 4, where comparisons between Lehane et al. (2022) (Eq. (6)) profiles and $q_{c.shallow}$ profiles from Kim et al. (2015) reveal systematic large deviations in the shallow failure zone. As was demonstrated in Fig. 2, the profiles by Kim et al. (2015) show good agreement in the shallow failure zone with both the theoretically derived model of Puech and Foray (2002) and the measured data by Krogh et al. (2022), further confirming the observed underestimation of $q_{c.shallow}$ with Lehane et al. (2022) profiles in natural deposits.

To improve agreement, an increase in $C_{2.shallow}$ from 3.2 to 3.8 is proposed (Table 1), and a slight adjustment to $f_{transition}$ (Eq. (9)) is similarly made; specifically, increasing n_1 to 0.6, while retaining $n_2 = 2$. As shown in Fig. 4 (profiles named 'this study'), these adjustments enable Eq. (6) to follow the upward concave portion of the Kim et al. (2015) profiles closely in the shallow failure penetration zone. The complete updated approach is summarized in the flow chart in Fig. 7, which is easily implemented in a spreadsheet. In the proposed approach, D_r is treated as a representative constant value, whereas curve fitting may be performed over selected depth intervals depending on the desired level of detail.

As shown in Fig. 8, curve fitting with the updated global model indicates $D_r \approx 0.5\text{-}0.7$ for CPT-02 (Fig. 8a) and $D_r \approx 0.6\text{-}0.8$ for CPT-03 (Fig. 8b), both in excellent agreement with the ND measurements ($D_r = 60\% \pm 10\%$ and $D_r = 80\% \pm 10\%$, respectively). The updated model achieves two key improvements: (1) it prevents convergence of the $q_{c.global}$ profiles in the surficial sand, allowing objective estimation of D_r; and (2) it yields strong agreement with the internal database, as demonstrated with numerous representative examples from the database later in this paper. Furthermore, the following section discusses cone size effects, in which the updated global model similarly show great performance with controlled tests by Iqbal (2002) and Larsen and Ibsen (2006).

The variability observed in the internal database is reflected in Table 3, which summarizes relative density interpretations for the upper 1 m of CPT data, using the updated global model. The descriptive categories from 'loose' to 'very dense' that are linked to the D_r values (see Table 3; descriptions correspond to interpretations from top to bottom of the upper 1 m profile) indicate substantial variation in the database.

5. Cone size effects

As embedded in Eq. (1) (Kim et al., 2015) and Eq. (4) (Puech and Foray, 2002), the cone diamater (d_c) plays an important role in the $q_{c.shallow}$ profiles. Specifically, an increase in d_c leads to a reduction in cone resistance at shallow failure penetration. By analysing CPT data obtained with varying cone diameters in uniform sand samples, Lehane et al. (2022) observed that data fall into a consistent trend when presented in a normalized chart, where the stress normalised cone resistance is plotted against the normalised penetration depth (z/d_c). This observation formed the basis for their $q_{c.shallow}$ profile expression (Eq. (6)), upon which the updated global model is an extension.

Essentially, Eq. (6) expresses a strong influence of cone diameter during shallow failure penetration, which diminishes with large penetration well into the deep failure penetration zone where profiles of varying d_c will eventually converge. This is consistent with experimental observations (e.g., Balachowski, 2007).

The updated global model is evaluated in Fig. 9 using CPTs conducted under controlled laboratory conditions by Iqbal (2002). The tests were performed with two significantly different cone diameters, $d_c = 1.13$ cm and $d_c = 3.57$ cm (standard field size cone), in fine to medium, uniformly graded silica sand. Three separate sand bodies with D_r ranging 0.62 to 0.84 were tested, with densities confirmed by direct measurements following uniform compaction using a vibration screen unit. As shown in Fig. 9, the updated global model exhibits excellent agreement with the measurements, remaining within about 5-10% (in absolute terms) of the measured values for both $d_c = 1.13$ cm and $d_c = 3.57$ cm in all three sand bodies.

Because shallow failure penetration is more pronounced in denser sand, the cone size effect is correspondingly greater. In contrast, shallow failure effects are minimal in loose sand. In Fig. 10, the global model is evaluated against a CPT with $d_c = 1.50$ cm performed in a loose, fine to medium, uniformly graded silica sand by Larsen and Ibsen (2006). Direct measurements indicated D_r ranging about 0.3 to 0.45. The sand specimen was prepared by water pluviation followed by minimal external vibration. Accordingly, a representative value of $K_0 = 0.5$, consistent with NC conditions, was assumed in the global model rather than using the recommended $K_0(z)$-procedure. Under these controlled conditions with minimal compaction disturbance, overconsolidation effects are expected to be negligible. As shown in Fig. 10, the global model again performs well, with curve fitting ranging about $D_r = 0.30\text{-}0.45$.

6. Case histories from the internal database

6.1 Onshore ground improvement

6.1.1 Site A

At a Danish onshore site, three CPTs (CPT-A1 to A3) using a standard 10 cm² cone and two nuclear densometer tests were conducted within a 15 m radius to assess compaction of a sand fill, see Fig. 11. Limiting void ratios of $e_{min} = 0.45$ and $e_{max} = 0.79$ were measured for the sand fill, typical for clean, subrounded to subangular silica sand (Youd, 1973). The ND tests are considered representative within the shallow failure zone, approximately the upper 0.45 m (Fig. 11a).

In this zone, D_r values with Eq. (3) ($D_{r.deep}$) are unreliable; therefore, ND data are used as the primary reference (Fig. 11b). The ND measurements yielded $D_r = 0.81$ and 0.87, indicating dense to very dense sand ($D_r \approx 0.84$) in the near-surface layer. Below this, D_r decreases to ~0.6 at a depth of 2 m, except in CPT-A3, where the sand fill ends at about 1.4 m.

Applying $D_r = 0.84$ in the updated global model results in $q_{c.global}$ profiles closely matching all three CPTs in the shallow zone (Fig. 11a). At greater depths, the measured CPT data diverge from $q_{c.global}$, consistent with the generally decreasing $D_{r.deep}$ profile (Fig. 11b), indicating that the compaction activities produced a denser sand deposit near the surface, which is not unusual of surface vibration compaction.

6.1.2 Site B

At a second Danish site (Site B), CPTs were performed using 10 cm² and 15 cm² cones (Table 2) to evaluate compaction of a medium to coarse sand fill. Particle size distribution (PSD) tests showed a uniformity coefficient (*UC*) ranging from 3 to 6, indicating minor local variations in gradation. These characteristics differ slightly from those of the uniformly graded sands ($UC \approx 2$) used in the development of the reference model.

Two example CPTs at Site B, conducted with a 10 cm² cone, are presented in Fig. 12 (CPT-B1, Fig. 12a; CPT-B2, Fig. 12b). As illustrated in Fig. 12c, the $D_{r.deep}$ profiles indicate that at CPT-B1, the relative density remains nearly constant with depth ($D_r \approx 0.65$–0.70), except in the shallow zone. In contrast, CPT-B2 shows a slight gradual increase in relative density with depth, from $D_r \approx 0.5$ to $D_r \approx 0.60$ at greater depths. Application of the updated global model (Figs. 12a and 12b) yields excellent agreement in the shallow zone, with estimated D_r values of 0.68 and 0.48, respectively. These results are consistent with the trends indicated by the $D_{r.deep}$ profiles in Fig. 12c, where indicative "corrected" values are provided for the shallow zone.

At Site B, 36 CPTs were carried out using a 15 cm² cone. These are the only tests in the internal database not performed with a 10 cm² cone and thus provide a valuable case for examining the applicability of the global model, although further validation is required to gain more confidence with this cone size. Two representative CPTs are shown in Fig. 13 (CPT-B3, Fig. 13a; CPT-B4, Fig. 13b). The $D_{r.deep}$ profiles (Fig. 13c) indicate that CPT-B3 is dominated by very dense sand ($D_r \approx 0.90$–0.95), except in the shallow zone. In contrast, CPT-B4 reveals two distinct layers: a medium-dense near-surface sand ($D_r \approx 0.60$) overlying a very dense layer ($D_r \approx 0.88$). Application of the updated global model (Figs. 13a and 13b) shows close agreement in the shallow zone, with estimated D_r values of 0.93 and 0.63, respectively, consistent with the $D_{r.deep}$ trends. The indicative "corrected" values shown in Fig 13c illustrate that the shallow zone increases with increasing relative density.

6.2 Offshore CPTs from the North Sea

Due to hydrostatic pore pressures, stress conditions during offshore CPTs differ from those in onshore tests, with the effective stresses typically being much lower. Figure 14 presents four offshore CPTs from the North Sea (Sites D and E, Table 2), where the upper layer consists of clean, uniformly graded siliceous sands (confirmed by sampling), illustrating a range of conditions. For clarity, the x-axis is plotted with a consistent scale across all charts in Fig. 14.

In Fig. 14a, the updated global model is applied to a CPT in loose sand within the top 1 m. Using D_r = 0.26, the $q_{c.global}$ profile reproduces the observed shape well and indicates only limited shallow failure (~0.1-0.2 m). By contrast, methods that assume deeper shallow failure (e.g., Emerson et al., 2008) would significantly overestimate D_r in this case.

Figure 14b shows a CPT in medium dense sand, where $q_{c.global}$ reflects D_r = 0.60. Figure 14c presents a near-uniform dense top layer (~1 m thick), with $q_{c.global}$ indicating $D_r \approx 0.77$ at the surface. In both cases, $D_{r.deep}$ would misclassify the deposits as loose to very loose in the near-surface.

In Fig. 14d, $q_{c.global}$ captures slight variations from dense to very dense sand within the upper ~1.5 m, with fitted D_r values ranging from ~0.7 to 0.9. Here again, $D_{r.deep}$ would misclassify the surficial sand as loose to very loose.

7. Discussion

The updated model builds on Jensen (2024), which was presented with an initial proof of concept calibration and emphasised the need for further calibration. Nevertheless, Jensen

(2024) demonstrated an improvement over existing approaches in capturing the realistic shape of shallow CPT profiles in sand. The shortcomings associated with the initial calibration are addressed in the present study through a recalibration based on previously published controlled laboratory tests and a large internal database of 132 CPTs compiled from industry projects.

As was demonstrated in Fig. 6, the initial Jensen (2024) model results in convergence of q_c profiles in the very shallow zone for certain ranges of D_r, preventing objective differentiation of D_r; this limitation is resolved with the updated model. Furthermore, the initial calibration tends to underestimate q_c in the shallow zone, with the discrepancy becoming increasingly pronounced with increasing D_r. This behaviour is illustrated in Fig. 15 through comparison of the initial calibration and the updated model using tests that were presented in Figs. 12 and 14. Overall, the updated model captures the shape of the q_c profiles more accurately, in agreement with the full internal database, and the difference between the initial and updated formulations increases with D_r.

Figure 16 presents a CPT in a sand deposit visually described as slightly silty to silty and possibly heavily overconsolidated due to past glacial activity. In this case, the updated global model underperforms near the surface, probably due to increased sand compressibility not represented in the model calibration. The shallow failure zone appears smaller than predicted by the global model, with deep failure initiating at ~0.3–0.4 m. This behavior is likely attributable to the fines content, although in other cases it may arise from angular particles, which increase compressibility while also enhancing dilatancy during shallow failure.

Figure 17 illustrates these effects: centrifuge CPTs in highly compressible, angular carbonate sand (Kwinana sand) and in moderately compressible silica sand (UWA sand), both at similar relative densities (D_r = 0.70 and 0.78), show that Kwinana sand develops higher shallow failure q_c ($q_{c.shallow}$) due to greater dilatancy from particle angularity, but lower q_c at deep failure penetration due to higher compressibility.

Discrepancies such as those in Fig. 16 could also reflect ageing, bonding, or cementation - factors not captured by the model, which was developed for young, unaged, clean sands. Similarly, intense man-made compaction activities can modify fabric and yield very high near-surface q_c values that are not reproduced by the model, necessitating careful engineering judgement when applying the global model at shallow depth.

The global model is more reliable for fully saturated or dry siliceous sands, as partially saturated conditions can compromise effective stress estimation due to pore pressure effects. Near the surface, particularly within the top 2-4 cone diameters, model reliability is increasingly affected by second-order effects and measurement sensitivity. In this shallow zone, factors such as precise mudline definition and minor cone disturbances can influence the estimated D_r. Improved methods for mudline identification are therefore recommended to enhance interpretation in the near-surface region.

The model is derived from clean, unaged, uncemented, moderately compressible siliceous sands. Application to sands with differing characteristics may introduce bias. A simple comparison of $D_{r.deep}$ estimates performed by the author, using the calibrations of Jamiolkowski et al. (2003) and Jensen (2024) (Table 1), applied to a database of 480 calibration chamber tests on 11 siliceous sands (compiled by Jefferies and Been, 2015), yielded standard deviations of 0.15 and 0.14, respectively, between measured and predicted D_r. These results support the general applicability of Jensen's (2024) calibration for $q_{c.deep}$ while also underscoring the uncertainties associated with D_r estimation, partly due to the inherent difficulty of defining limiting void ratios (Lunne et al., 2019).

8. Conclusion

This paper has critically reviewed existing approaches for estimating relative density (D_r) from shallow depth CPTs in sands and presented an updated global model that unifies shallow and deep failure mechanisms, calibrated against CPTs performed under controlled laboratory testing and a comprehensive internal database of 132 onshore and offshore CPTs. The main conclusions are:

1. Advancement beyond Jensen (2024)
    - The updated calibration refines the shallow penetration formulation and transition function proposed in Jensen (2024), enabling more objective differentiation of D_r in the shallow zone.
    - The revised model reduces shallow-zone bias and provides improved agreement with measured q_c profiles across a substantially expanded dataset.
2. Validation
    - The model has been evaluated against numerous controlled laboratory tests, by comparison with alternative theoretical and empirical approaches, and an extensive internal database of 132 suitable CPTs from onshore and offshore sites, covering a broad range of conditions.
    - Validation is primarily based on tests with the most widely used 10 cm² cone, which represents the current basis of calibration. While controlled laboratory testing as well as the limited number of tests with 15 cm² cones show

    promising agreement, further validation is required before general application across cone sizes.
  - Case studies confirm strong agreement with independent direct relative density measurements.

3. Applicability and limitations
   - The model is most reliable for clean, young, uncemented, uniformly graded siliceous sands under fully saturated or dry conditions.
   - Shortcomings are illustrated for sands with higher compressibility where factors such as fines content and very angular particle shape may alter the penetration response beyond the calibrated range.
   - Within the upper 2-4 cone diameters, reliability decreases due to mudline definition and cone disturbance effects, reinforcing the need for improved mudline definition method.
4. Recommendations for practice
   - As natural soils rarely exhibit idealized behaviour, site-specific validation of the model against direct D_r measurements is required, even when soils appear to fall within the calibrated range of the model.
   - Engineering judgement is required to assess potential effects of ageing, bonding, cementation, or intense man-made compaction, where soil fabric effects can produce very high near-surface q_c values not reproduced by the model.
   - Future work could focus on extending calibration to a wider variety of sands (including angular and highly compressible types), further validating across cone sizes, and improving mudline identification methods for shallow penetration analysis.

Acknowledgements

The author gratefully acknowledges Geo for granting permission to compile and use the database drawn from internal projects for this paper.

Funding Statement: There is no funding to report for this submission.

Competing Interests Statement: The author declares there are no competing interests.

Data Availability Statement: Data generated or analysed during this study are not available due to confidentiality.

References

Agaiby, S. S., and Mayne, P. W. (2019). CPT Evaluation of Yield Stress Profiles in Soils. *J. Geotech. Geoenviron. Eng.*, 145(4), 04019104. *https://doi.org/10.1061/(ASCE)GT.1943-5606.0002164*

Arshad, M. I., Tehrani, F. S., Prezzi, M., and Salgado, R. (2014). Experimental study of cone penetration in silica sand using digital image correlation. *Géotechnique*, 64 (7), 551-569. *https://doi.org/10.1680/geot.13.P.179*

Balachowski, L. (2007). Size effect in centrifuge cone penetration tests. *Arch. Hydro-eng. Environ. Mech.,* 54 (3), 161-181.

Baldi, G., Bellotti, R., Ghiona, V., Jamiolkowski, M., & Pasqualini, E. (1986). Interpretation of CPTs and CPTUs. Part II: drained penetration of sands. In *Proc., 4th International Geotechnical Seminar on Field Instrumentation and in situ Measurements*, 143-156. Nanyang Technological Institute, Singapore.

Biarez, J., & Gresillon, J. M. (1972). Essais et suggestions pour le calcul de la force portante des pieux en milieu pulvérulent. *Géotechnique*, 22 (2), 433-450. *https://doi.org/10.1680/geot.1972.22.3.433*

Bolton, M. D., Gui, M. W., Garnier, J., Corte, J. F., Bagge, G., Laue, J., & Renzi, R. (1999). Centrifuge cone penetration tests in sand. *Géotechnique*, 49 (4), 543-552. *https://doi.org/10.1680/geot.1999.49.4.543*

Durgunoglu, H. T., & Mitchell, J. K. (1973). Static penetration resistance of soils. In Proc., *8th Int. Conf. on Soil Mechanics and Foundation Engineering*, 1, 243–247. Moscow, USSR.

El-Sekelly, W., Tessari, A., & Abdoun, T. (2015). Effect of overconsolidation on K_o in centrifuge models using CPT and tactile pressure sensor. *Geotechnical Testing Journal*, 38(1), 1–12. *https://doi.org/10.1520/GTJ20140086*

Emerson, M., Foray, P., Puech, A., & Palix, E. (2008). A global model for accurately interpreting CPT data in sands from shallow to greater depth. *In proc., Geotechnical and Geophysical Site Characterisation – the third international conference on site characterization*. Taylor & Francis Group, London. pp. 687–694.

Houlsby, G. T., & Hitchman, R. (1988). Calibration chamber tests of a cone penetrometer in sand. *Geotechnique*, 38 (1), 39–44. *https://doi.org/10.1680/geot.1988.38.1.39*

Iqbal, Z. (2002). Shallow Cone Penetration Tests in Sand: Analysis of Penetration Tests using Different Cones, CBR Plunger & Plate. M.Sc. Thesis H.E. 118, International Institute for Infrastructural, Hydraulic and Environmental Engineering (IHE Delft), Delft, The Netherlands.

Jamiolkowski, M., Presti, D. C., & Manassero, M. (2003). Evaluation of relative density and shear strength of sands from cone penetration test (CPT) and flat dilatometer (DMT). In Germaine, J. T., Sheahan, T. C., and Whitman, R. V. (Eds.), *Soil Behavior and Soft*

Ground Construction, ASCE Geotechnical Special Publication, 119. American Society of Civil Engineers (ASCE), 201–238.

Jefferies, M., & Been, K. (2015). Soil Liquefaction: A Critical State Approach, Second Edition. Soil Liquefaction: a Critical State Approach, Second Edition (pp. 1–677). CRC Press. *https://doi.org/10.1201/b19114*

Jensen, M. R. (2024). Estimating relative density from shallow depth CPTs in normally consolidated and overconsolidated siliceous sand. *Canadian Geotechnical Journal*, 62, 1–14. *https://doi.org/10.1139/cgj-2024-0136*

Kim, J. H., Choo, Y. W., Kim, D. J., & Kim, D. S. (2015). Miniature Cone Tip Resistance on Sand in a Centrifuge. *J. Geotech. Geoenviron. Eng.*, 142 (3), 591–602. *https://doi.org/10.1061/(ASCE)GT.1943-5606.0001425*

Konrad, J.-M. (1998). Sand state from cone penetration tests: a framework considering grain crushing stress. Geotechnique, 48(2), 201–215. *https://doi.org/10.1680/geot.1998.48.2.201*

Krogh, L., Quinteros, S., Engin, H. K., & Lunne, T. (2022). Revisiting interpretation of relative density from shallow depth CPTs in sand. *Canadian Geotechnical Journal*, 59 (6), 808–826. *https://doi.org/10.1139/cgj-2021-0200*

Larsen, K. A., & Ibsen, L. B. (2006). Method for Predicting Void Ratio and Triaxial Friction Angle from Laboratory CPT at Shallow Depths. Department of Civil Engineering, Aalborg University. AAU Geotechnical Engineering Papers No. R0608

Lehane, B. M., Zania, V., Chow, S. H., & Jensen, M. (2022). Interpretation of centrifuge CPT data in normally consolidated silica and carbonate sands. *Geotechnique*, 73 (10), 907–916. *https://doi.org/10.1680/jgeot.21.00177*

Liu, Q., & Lehane, B. M. (2020). A centrifuge investigation of the relationship between the vertical response of footings on sand and CPT end resistance. *Géotechnique*, 70(5), 455–465. *https://doi.org/10.1680/jgeot.19.P.253*

Lunne, T., Knudsen, S., Blaker, Vestgården, T., Powell, J. J. M., Wallace, C. F., … Ghanekar, R. K. (2019). Methods used to determine maximum and minimum dry unit weights of sand: Is there a need for a new standard? Canadian Geotechnical Journal, 56(4), 536–553. *https://doi.org/10.1139/cgj-2017-0738*

Puech, A., & Foray, P. (2002). Refined Model for Interpreting Shallow Penetration CPTs in Sands. In *Proc., Annual Offshore Technology Conference*, OTC 14275.

Richards, I. A., Bransby, M. F., Byrne, B. W., Gaudin, C., & Houlsby, G. T. (2021). Effect of Stress Level on Response of Model Monopile to Cyclic Lateral Loading in Sand. *Journal of Geotechnical and Geoenvironmental Engineering*, 147(3). *https://doi.org/10.1061/(ASCE)GT.1943-5606.0002447*

Roy, A. (2020). Numerical and experimental investigation of plate anchor capacity in sand. PhD thesis, The University of Western Australia. *https://doi.org/10.26182/dfd0-w151*

Salgado, R., & Prezzi, M. (2007). Computation of Cavity Expansion Pressure and Penetration Resistance in Sands. *International Journal of Geomechanics*, 7 (4), 251–265. *https://doi.org/10.1061/(ASCE)1532-3641(2007)7:4(251)*

Schmertmann, J.H. (1976). An Updated Correlation between Relative Density D_R and Fugro-Type Electric Cone Bearing, q_c. Contract Report DACW 39-76 M 6646 WES, Vicksburg, Miss., 1976.

Schmertmann, J.H. (1978). Guidelines for Cone Penetration Test: Performance and Design. Washington, D.C., Report FHWA-TS-78-209.

Youd, T. L. (1973). Factors controlling maximum and minimum densities of sands. In *Evaluation of Relative Density and Its Role in Geotechnical Projects Involving*

Cohesionless Soils (pp. 98–112). ASTM Special Technical Publication No. 523. American Society for Testing and Materials. *https://doi.org/10.1520/STP37866S*

Yu, H. S., & Mitchell, J. K. (1998). Analysis of cone resistance: Review of methods. *Journal of Geotechnical and Geoenvironmental Engineering*, 124 (2), 140–149. *https://doi.org/10.1061/(ASCE)1090-0241(1998)124:2(140)*

Table 1. Calibration parameters for $q_{c.deep}$ (Eq. (2)) and $q_{c.shallow}$ (Eq. (6)) for various references.

Reference	Deep ($\sigma' = p'$)			Shallow ($\sigma' = \sigma'_v$)		
	$C_{0.deep}$	$C_{1.deep}$	$C_{2.deep}$	$C_{0.shallow}$	$C_{1.shallow}$	$C_{2.shallow}$
Jamiolkowski et al. (2003)	24.94	0.46	2.96	-	-	-
Lehane et al. (2022)	-	-	-	19	0.7	3.2
Jensen (2024)	25.6	0.7	3.2	19	0.7	3.2
This study	25.6	0.7	3.2	19	0.7	3.8

Table 2. Details of the internal CPT database

Site	No. of tests	Cone size	Geography	Offshore/ onshore	General sand description
A	3	10 cm^2	Denmark	Onshore	Sand fill, siliceous, clean, medium, uniform
B-1	24	10 cm^2	Denmark	Onshore	Sand fill, siliceous, clean, medium to coarse, uniform to well graded
B-2	36	15 cm^2	Denmark	Onshore	Sand fill, siliceous, clean, medium to coarse, uniform to well graded
C	6	10 cm^2	Germany	Onshore	Siliceous, clean, fine to medium, uniform
D	3	10 cm^2	North Sea	Offshore	Post-glacial, siliceous, clean, fine to coarse, uniform
E	1	10 cm^2	North Sea	Offshore	Post-glacial, siliceous, clean, fine, uniform
F	12	10 cm^2	North Sea	Offshore	Post-glacial, siliceous, clean, fine to medium, uniform
G	10	10 cm^2	North Sea	Offshore	Post-glacial, siliceous, clean, fine to medium, uniform
H	37	10 cm^2	Irish Sea	Offshore	Siliceous (no detailed sample descriptions)

Table 3. Summary of interpreted D_r within the upper 1 m of CPT data from the internal database, based on the updated global model. Descriptions correspond to interpretations from top to bottom of the 1 m profile, with numbering indicating the count of CPTs in each category.

Interpretation[1]	Site								
	A	B-1	B-2	C	D	E	F	G	H
Loose	-	-	-	-	1	-	2	1	3
Loose to medium dense	-	1	-	-	-	-	-	1	4
Loose to dense	-	-	-	-	-	-	-	2	-
Medium dense	-	7	1	-	1	-	1	2	12
Medium dense to dense	-	4	-	3	-	-	1	2	4
Medium dense to very dense	-	-	-	-	-	-	4	-	2
Dense to medium dense	-	-	-	-	-	-	-	-	8
Dense	1	12	1	1	1	-	1	1	4
Dense to very dense	-	-	-	2	-	1	3	1	-
Very dense to medium dense	1	-	-	-	-	-	-	-	-
Very dense to dense	1	-	2	-	-	-	-	-	-

[1] *Very loose: D_r = 0-0.15, Loose: D_r = 0.15-0.35, Medium dense: D_r = 0.35-0.65, Dense: 0.65-0.85, Very dense: D_r = 0.85-1*

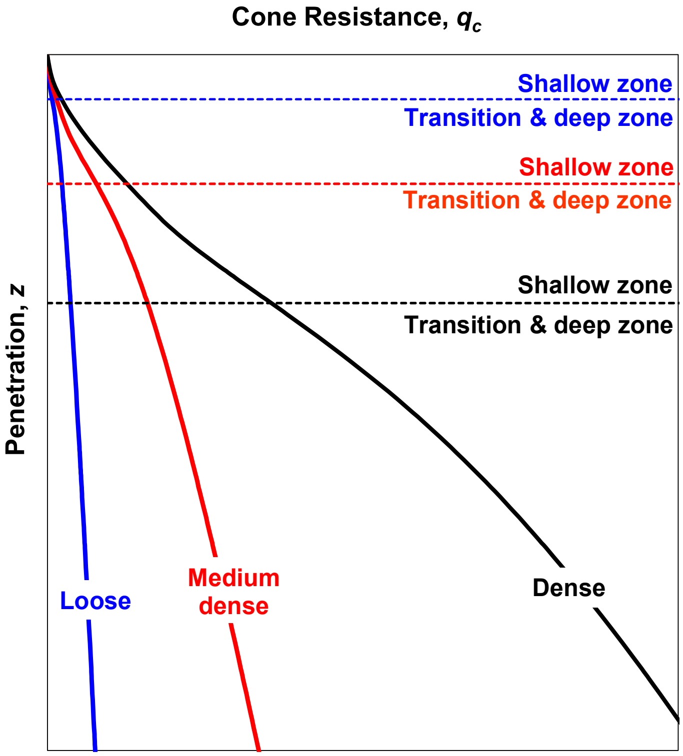

Fig. 1. Idealized shallow depth cone resistance profiles in uniform loose, medium dense, and dense sand.

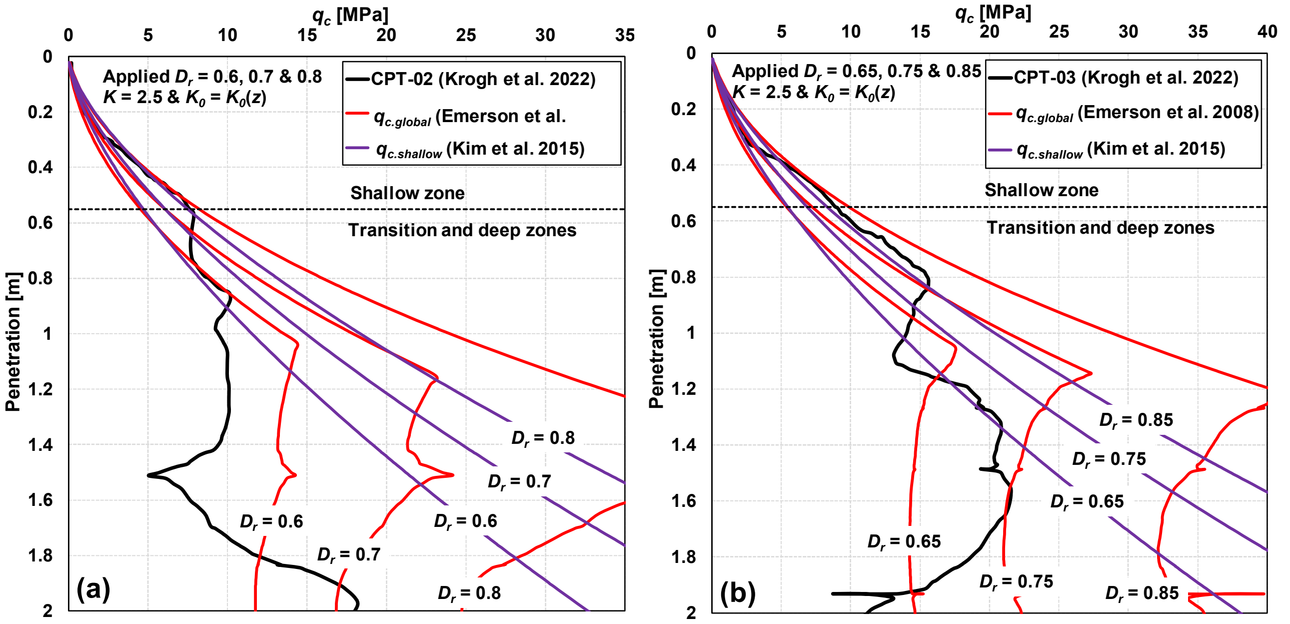

Fig. 2. Performance of Emerson et al. (2008) for shallow depth interpretation in siliceous sand compared with Kim et al. (2015). (a) CPT-02 (Krogh et al. 2022): measured q_c profile compared with $q_{c.global}$ (Emerson et al. 2008) and $q_{c.shallow}$ (Kim et al., 2015) for $D_r = 0.6$-0.8 ($K = 2.5$, $K_0 = K_0(z)$). (b) CPT-03 (Krogh et al. 2022): measured q_c profile compared with $q_{c.global}$ (Emerson et al. 2008) and $q_{c.shallow}$ (Kim et al. 2015) for $D_r = 0.65$–0.85 ($K = 2.5$, $K_0 = K_0(z)$).

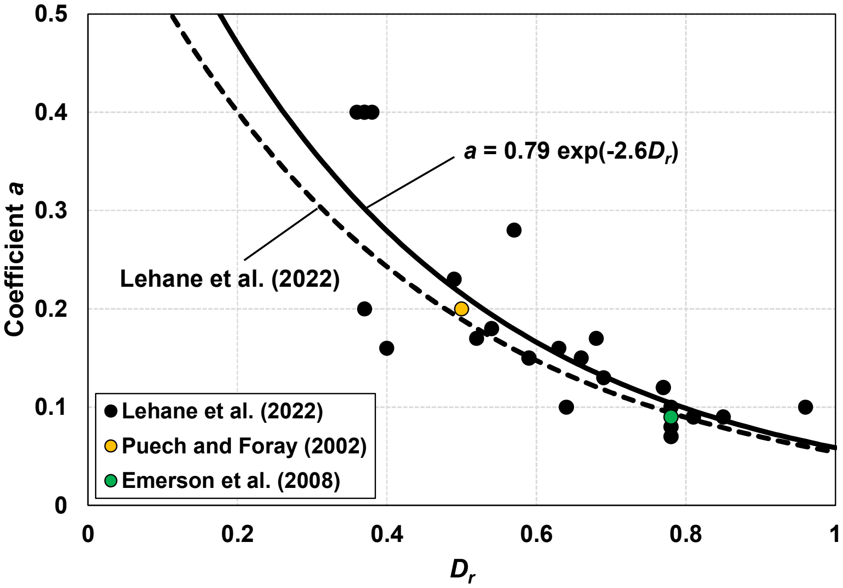

Fig. 3. Variation of coefficient *a* with D_r, showing data from Lehane et al. (2022), values inferred from data of by Puech and Foray (2002) and Emerson et al. (2008), and the updated expression proposed in this study (Eq. (10)).

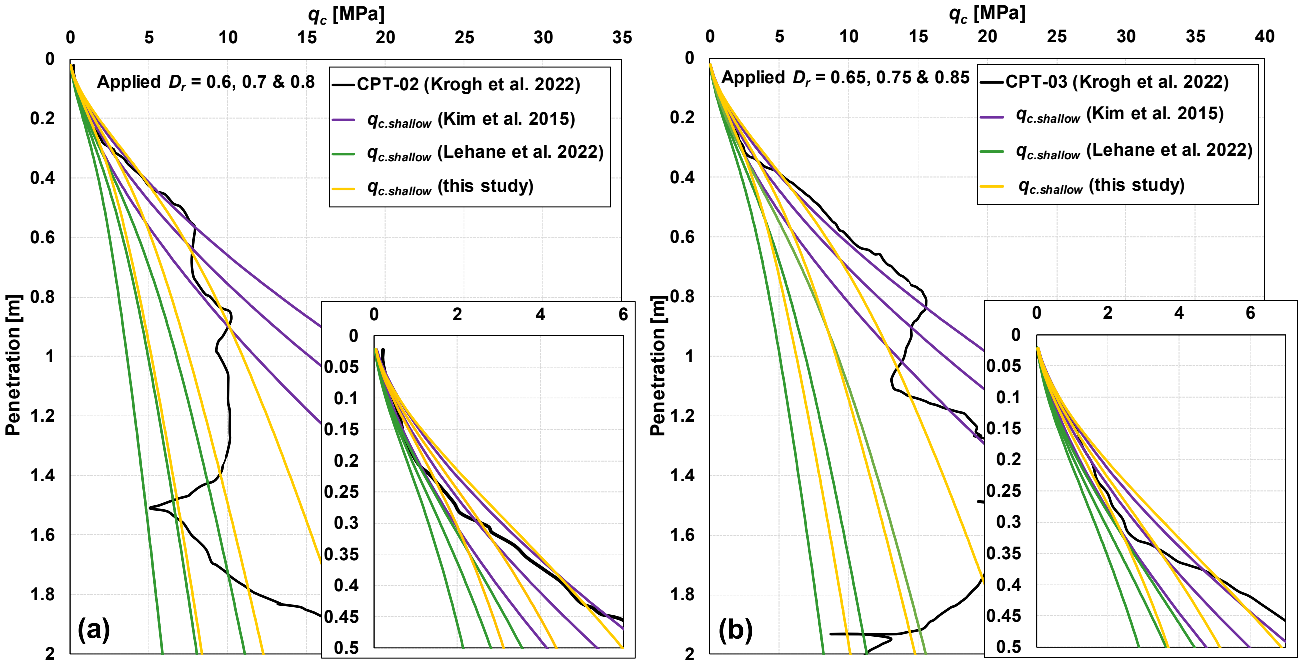

Fig. 4. Comparison of shallow penetration formulations in siliceous sand for CPT-02 and CPT-03 (Krogh et al. 2022). (a) CPT-02: measured q_c compared with $q_{c.shallow}$ from Kim et al. (2015), Lehane et al. (2022), and the modified formulation proposed in this study for D_r = 0.6-0.8. (b) CPT-03: measured q_c compared with $q_{c.shallow}$ from Kim et al. (2015), Lehane et al. (2022), and the modified formulation proposed in this study for D_r = 0.65-0.85.

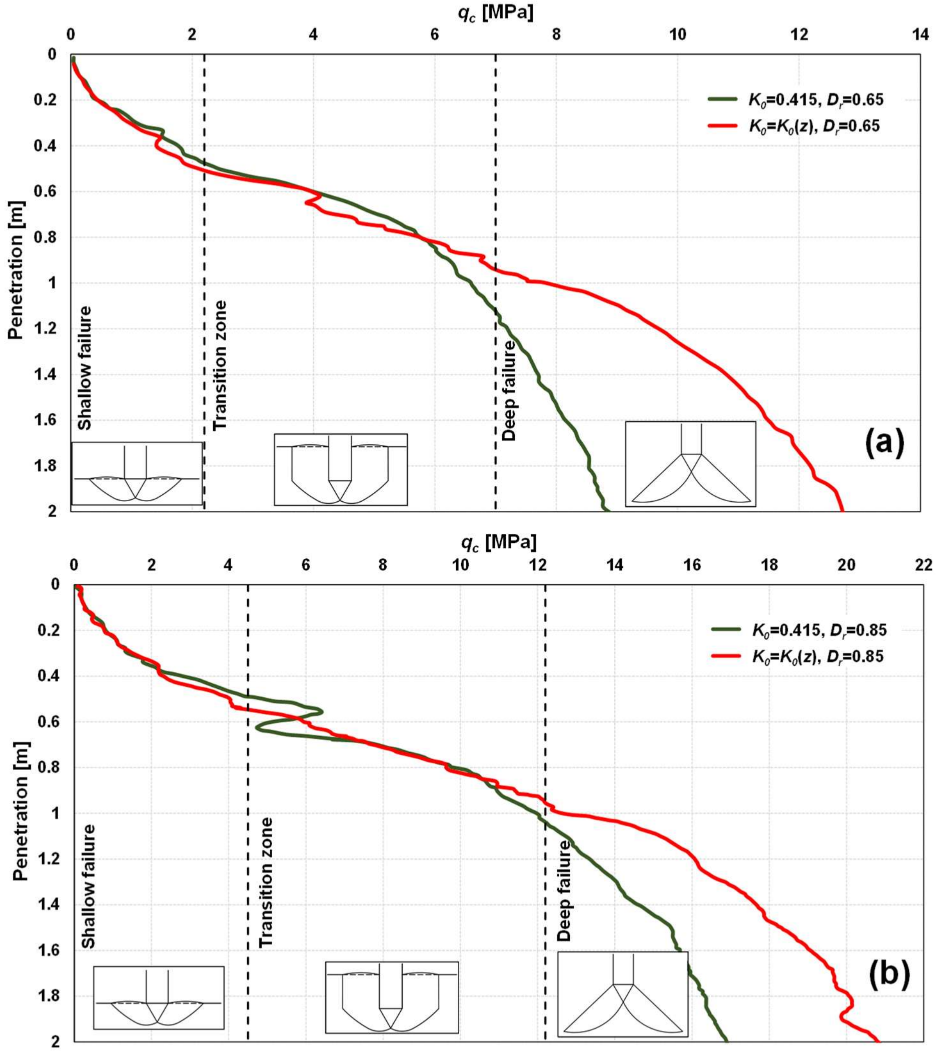

Fig. 5. Numerical simulations by Krogh et al. (2022) illustrating shallow and deep penetration mechanisms. (a) $D_r = 0.65$: comparison of q_c profiles for constant $K_0 = 0.415$ and depth-dependent $K_0(z)$. (b) $D_r = 0.85$: comparison of q_c profiles for constant $K_0 = 0.415$ and depth-dependent $K_0(z)$.

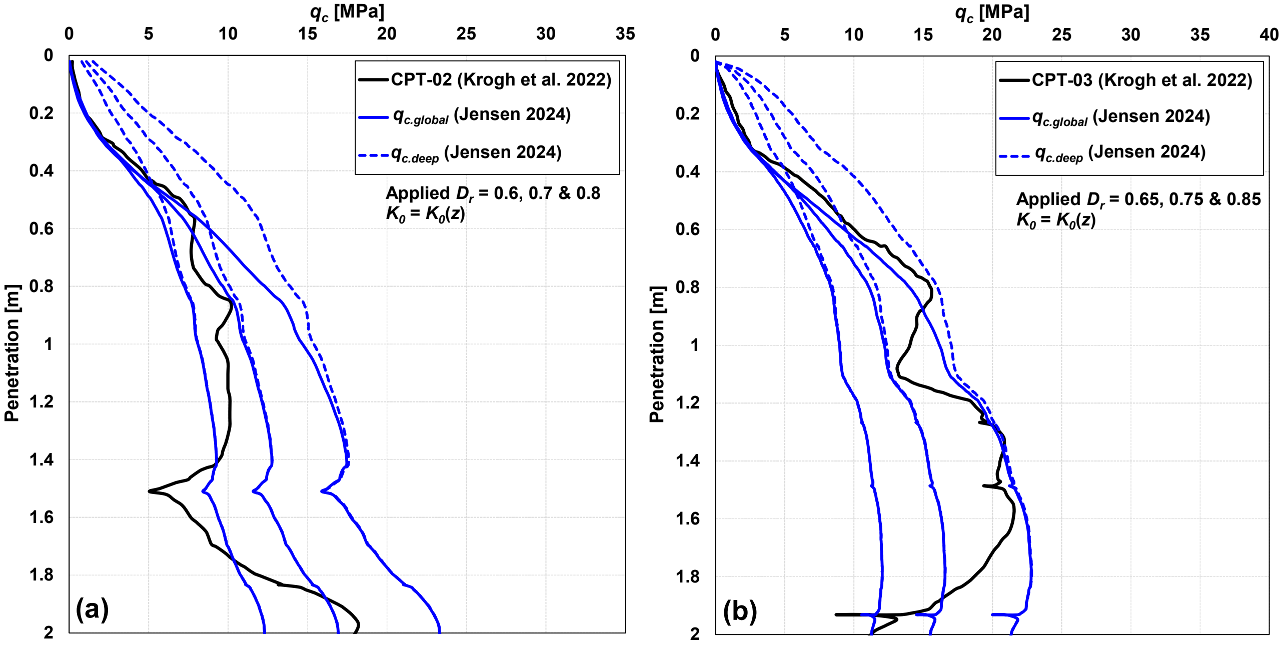

Fig. 6. Performance of Jensen (2024) global model for shallow depth interpretation in siliceous sand. (a) CPT-02 (Krogh et al. 2022): measured q_c compared with $q_{c.global}$ and $q_{c.deep}$ for D_r = 0.6-0.8 using $K_0 = K_0(z)$. (b) CPT-03 (Krogh et al. 2022): measured q_c compared with $q_{c.global}$ and $q_{c.deep}$ for D_r = 0.65-0.85 using $K_0 = K_0(z)$.

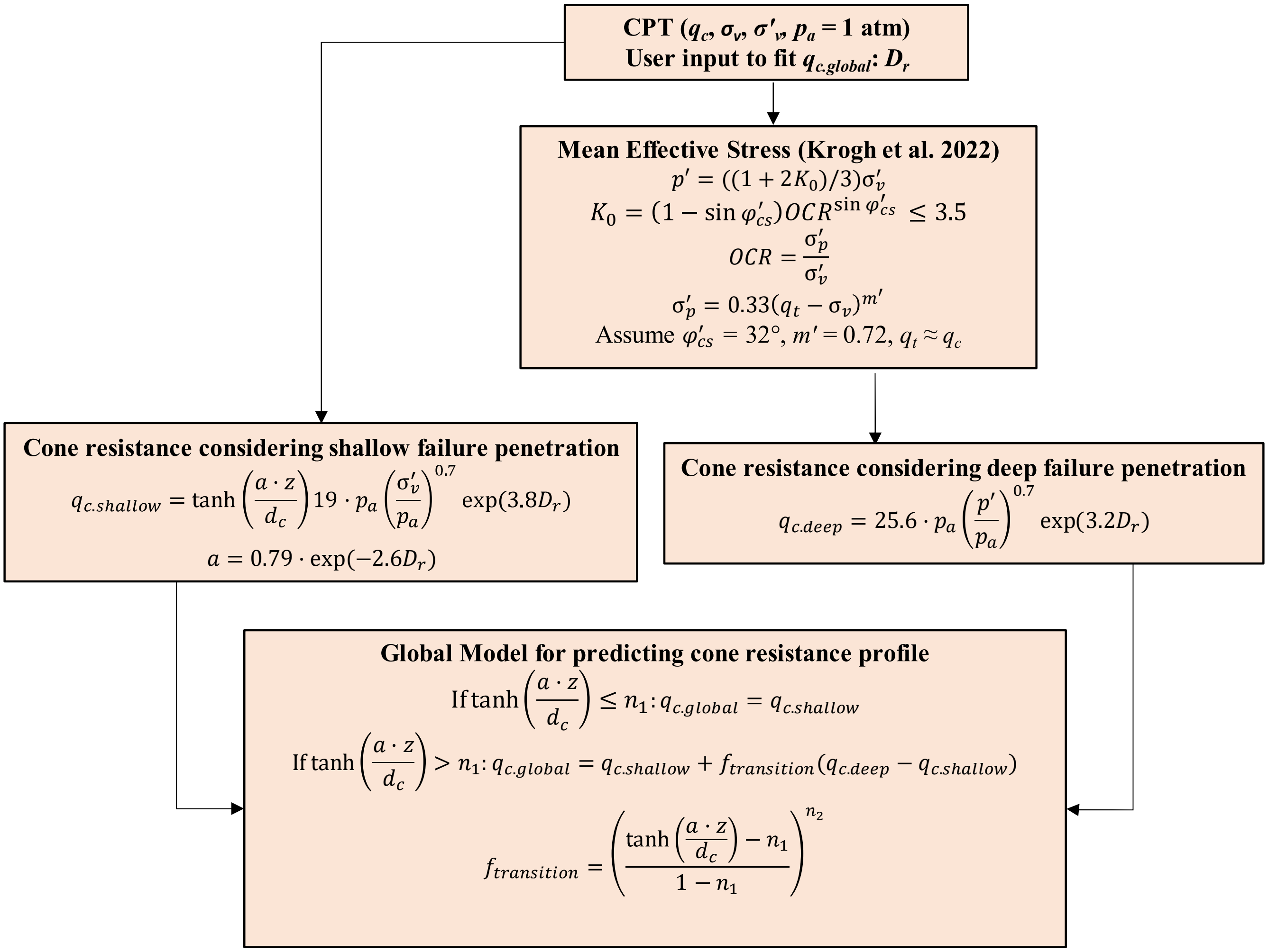

Fig. 7. Flow chart summarizing the updated global model for interpretation of shallow depth CPTs in siliceous sand. The CPT input parameters include cone resistance (q_c), vertical total stress (σ_v), vertical effective stress (σ'_v), and reference stress ($p_a = 100$ kPa). The corrected cone resistance is denoted q_t. The preconsolidation stress is σ'_p, the overconsolidation ratio is OCR, and m′ is an empirical stress exponent. The transition parameters are suggested as $n_1 = 0.6$ and $n_2 = 2$.

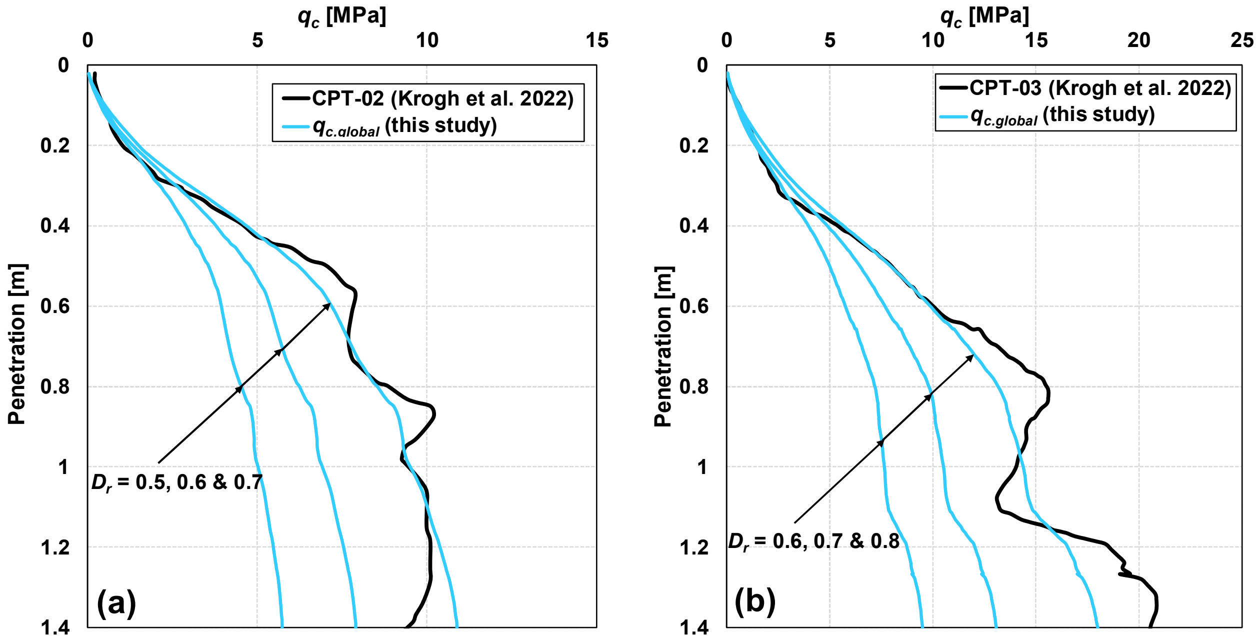

Fig. 8. Performance of updated global model ($q_{c.global}$) for CPTs from Krogh et al. (2022). (a) CPT-02: measured q_c compared with $q_{c.global}$ for D_r = 0.5–0.7. (b) CPT-03: measured q_c compared with $q_{c.global}$ for D_r = 0.6–0.8.

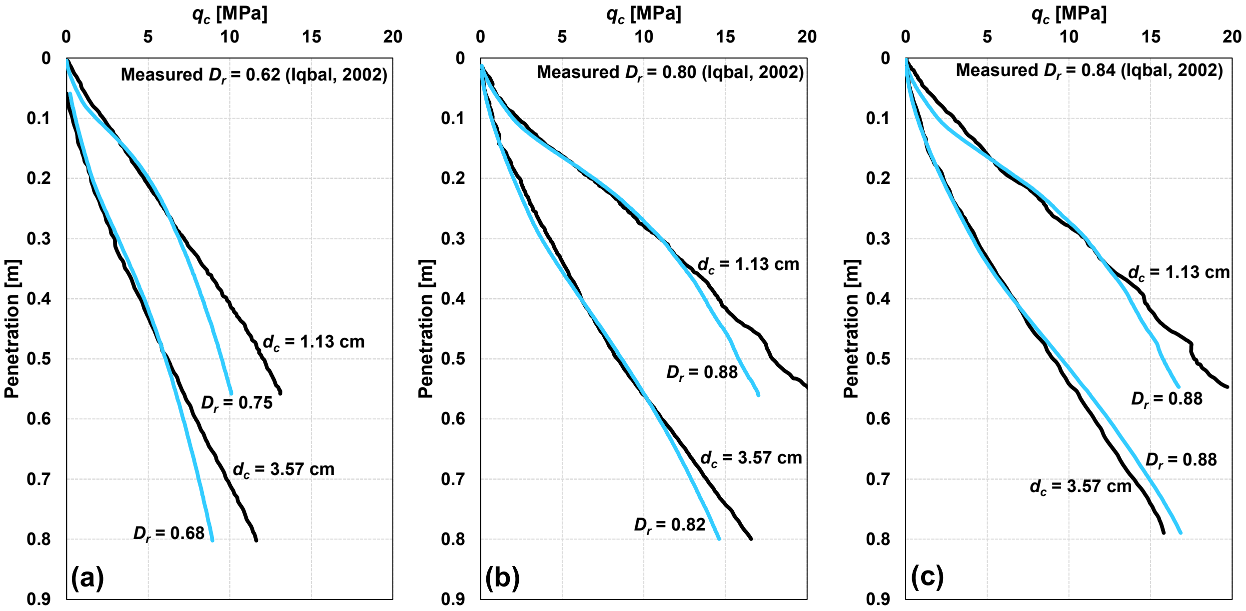

Fig. 9. Evaluation of the updated global model ($q_{c.global}$) against laboratory CPT data from Iqbal (2002), illustrating cone size effects in uniformly graded silica sand. (a) Sand body 1: measured q_c for d_c = 1.13 cm and d_c = 3.57 cm compared with $q_{c.global}$ for corresponding D_r values. (b) Sand body 2: measured q_c for d_c = 1.13 cm and d_c = 3.57 cm compared with $q_{c.global}$. (c) Sand body 3: measured q_c for d_c = 1.13 cm and d_c = 3.57 cm compared with $q_{c.global}$.

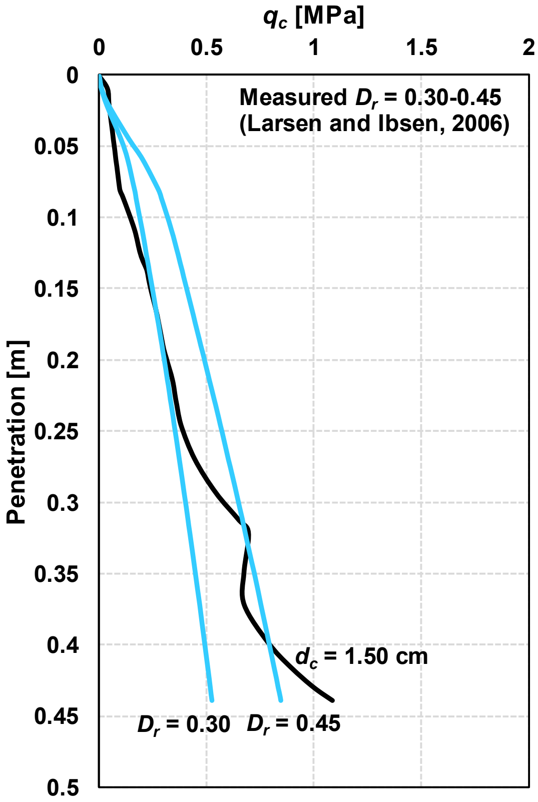

Fig. 10. Comparison between measured and predicted cone resistance profiles from Larsen and Ibsen (2006) in loose, uniformly graded silica sand (d_c = 1.50 cm), showing performance of the updated global model ($q_{c.global}$) assuming K_0 = 0.5.

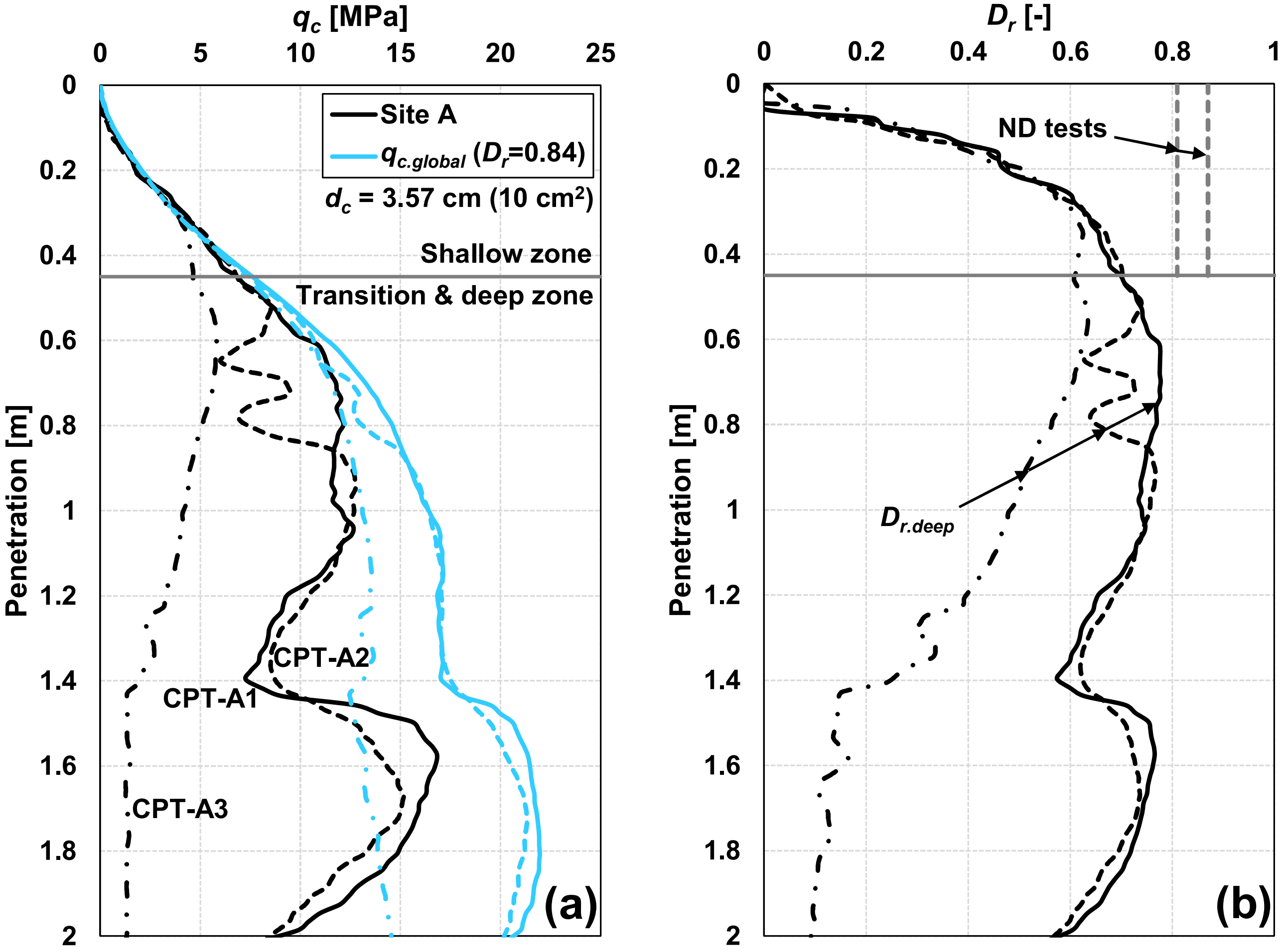

Fig. 11. CPT interpretation at Site A (onshore sand fill). (a) Measured q_c profiles (CPT-A1 to A3) compared with $q_{c.global}$ for $D_r \approx 0.84$ in the shallow zone. (b) Relative density profiles: comparison between $D_{r.deep}$ and nuclear densometer (ND) measurements.

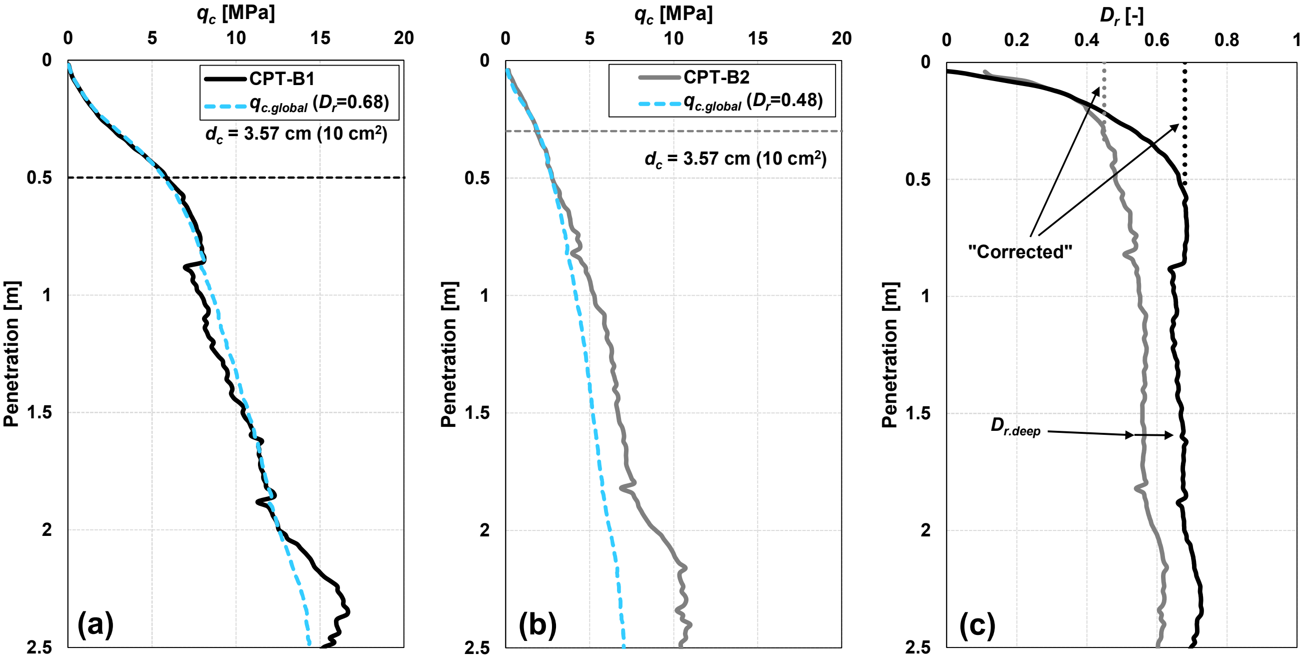

Fig. 12. CPT interpretation at Site B using 10 cm² cone. (a) CPT-B1: measured q_c compared with $q_{c.global}$; shallow $D_r \approx 0.68$. (b) CPT-B2: measured q_c compared with $q_{c.global}$; shallow $D_r \approx 0.48$. (c) Corresponding $D_{r.deep}$ profiles and indicative corrected shallow D_r values.

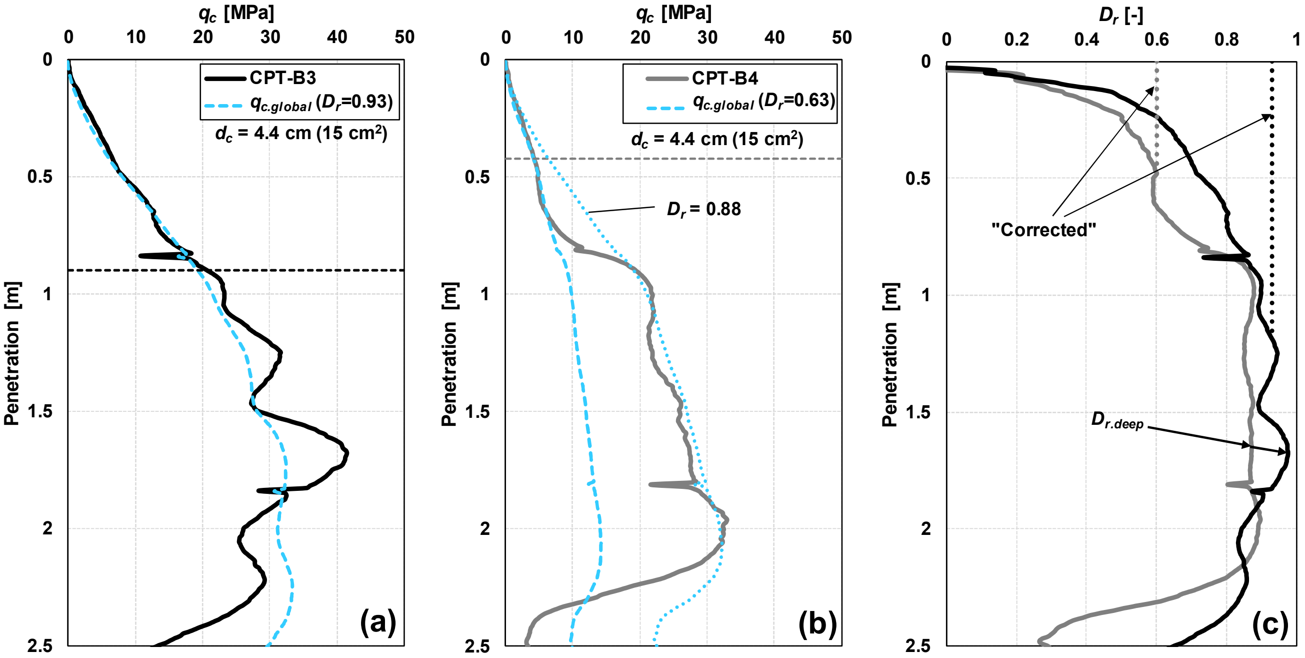

Fig. 13. CPT interpretation at Site B using 15 cm² cone. (a) CPT-B3: measured q_c compared with $q_{c.global}$; shallow $D_r \approx 0.93$. (b) CPT-B4: measured q_c compared with $q_{c.global}$; shallow $D_r \approx 0.63$. (c) Corresponding $D_{r.deep}$ profiles illustrating density variation with depth.

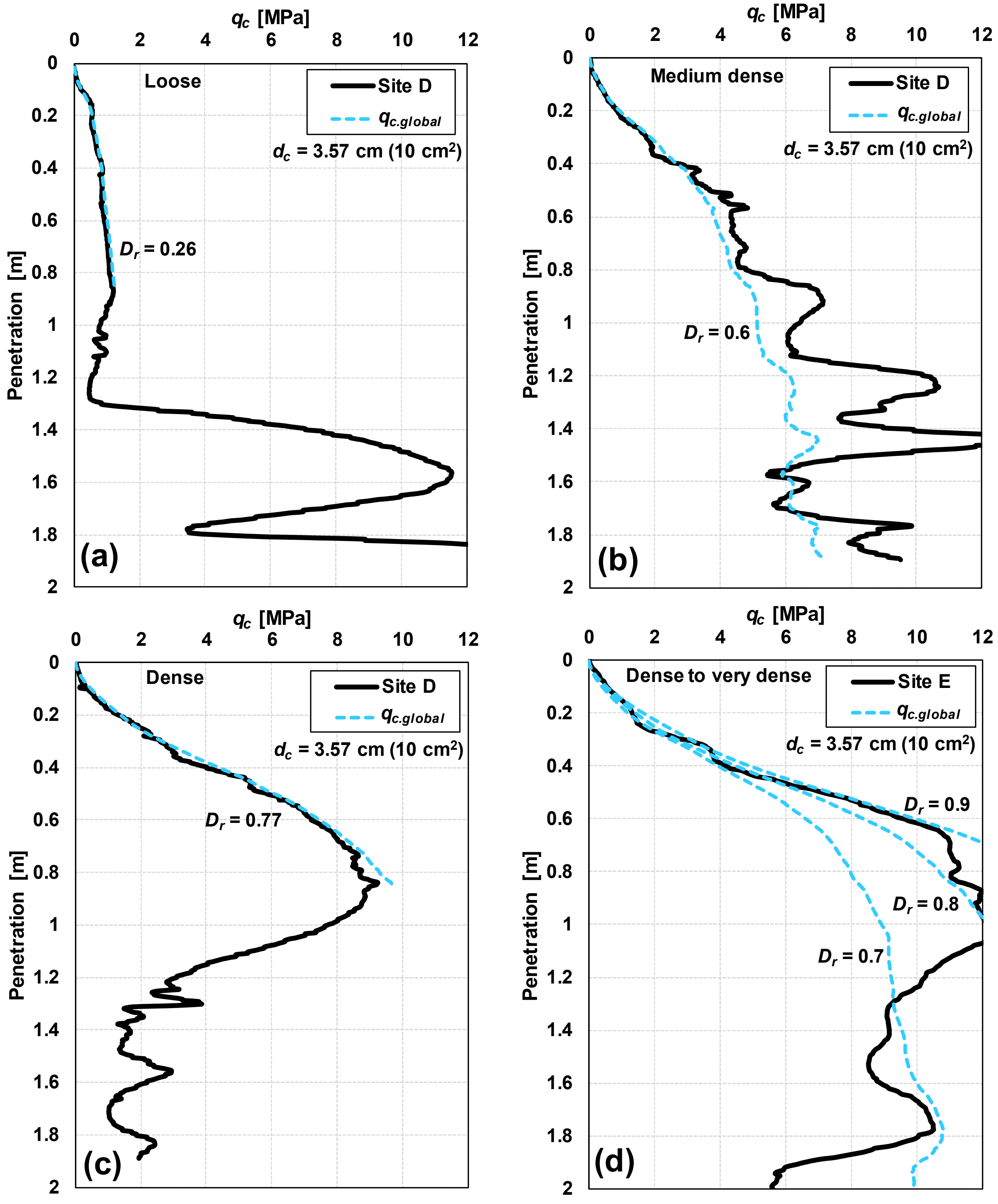

Fig. 14. Offshore CPTs from the North Sea illustrating shallow depth interpretation using the updated global model. (a) Loose sand ($D_r \approx 0.26$). (b) Medium dense sand ($D_r \approx 0.60$). (c) Dense near-surface sand layer ($D_r \approx 0.77$). (d) Dense to very dense sand with slight vertical variability ($D_r \approx 0.7$–0.9).

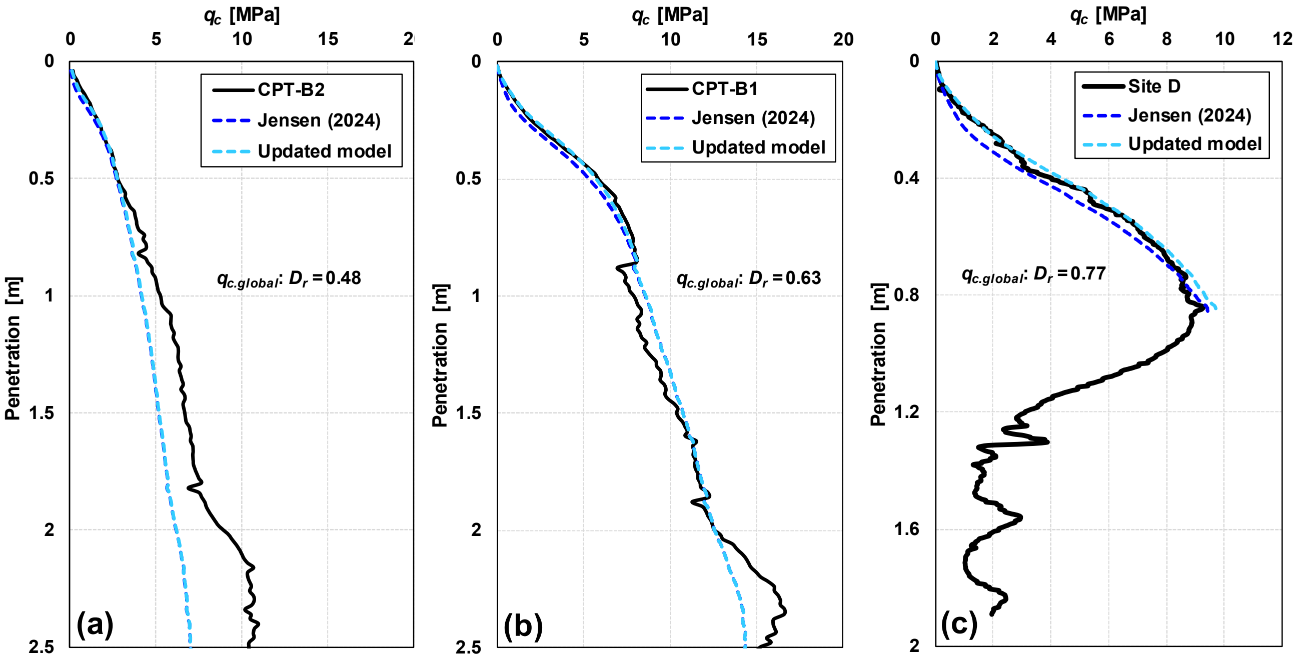

Fig. 15. Comparison between Jensen (2024) global model and the updated model. (a) CPT-B2; $q_{c.global}$: $D_r = 0.48$. (b) CPT-B1; $q_{c.global}$: $D_r = 0.63$. (c) Site D; $q_{c.global}$: $D_r = 0.77$.

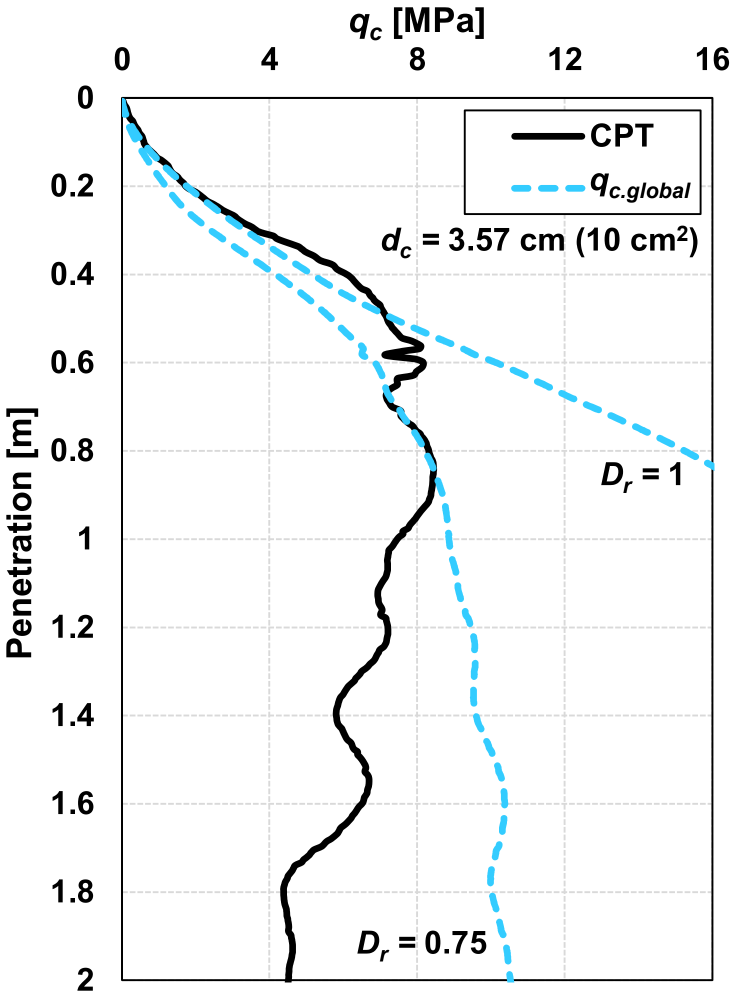

Fig. 16. Example application with poor performance of updated global model ($q_{c.global}$) for an offshore CPT from the North Sea.

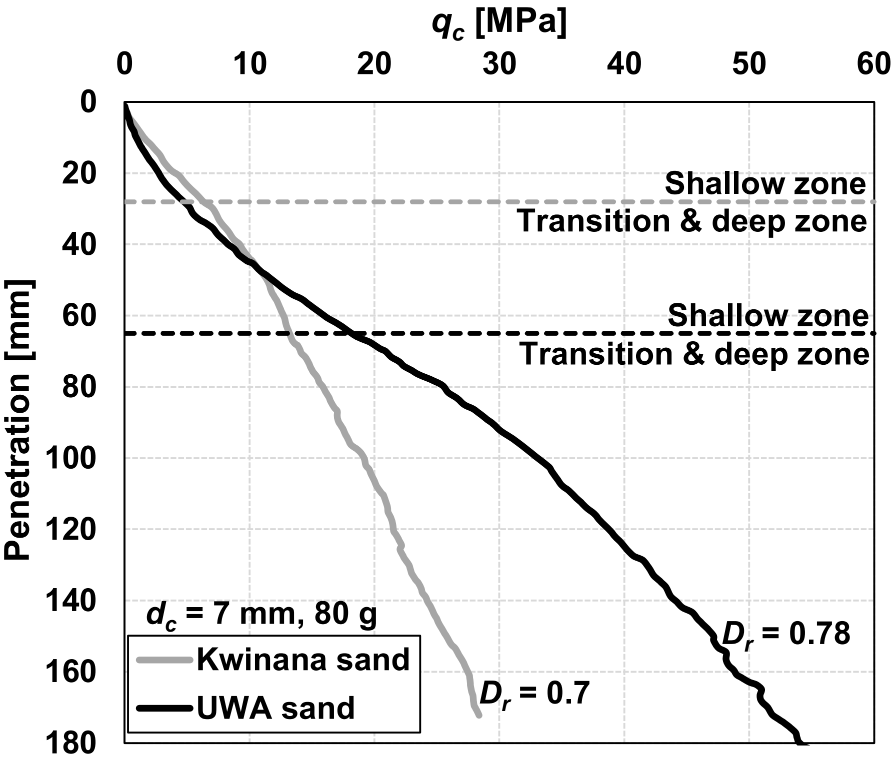

Fig. 17. Centrifuge CPTs in a high compressibility carbonate sand (Kwinana sand) and a moderately compressible sand (UWA sand) (measured data from Liu and Lehane, 2020).